CONF-900140--4

UCRL--102275

DE90 006263

UCRL- 102275
PREPRINT

Performance of a 500 Watt Nd:GGG Zigzag Slab Oscillator

L. Zapata
K. Manes
D. Christie
J. Davin
J. Blink
J. Penland
R. Demaret
G. Dallum

This paper was prepared for submittal to
SPIE
Los Angeles, CA
January 14-19, 1990

January 12, 1990

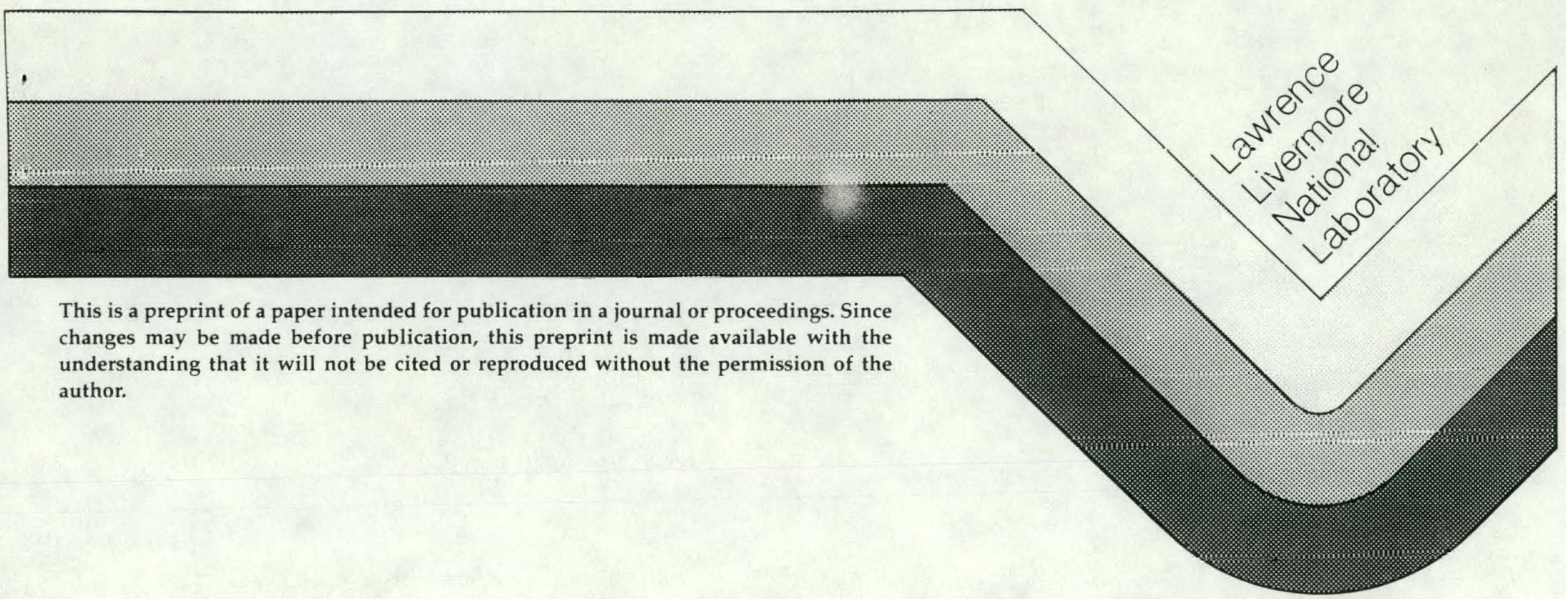

DISCLAIMER

DISCLAIMER

Performance of a 500 watt Nd:GGG zigzag slab oscillator

L. E. Zapata, K. R. Manes, D. Christie, J. Davin, J. Blink,
J. Penland, R. Demaret, and G. Dallum.

Lawrence Livermore National Laboratory
Livermore, CA 94550

ABSTRACT

Realization of practical multi-kilowatt Nd:garnet lasers will require the scale-up of crystal dimensions as well as more powerful pumping sources. A high average power zigzag slab crystal amplifier testing facility has been established at LLNL which employs two 100 kW_e vortex stabilized arc lamps, cooled reflectors and a cooled, spectrally filtered, crystal slab mounting fixture. The operational characteristics of the first crystal laser to be tested in this setup, a Nd:GGG zigzag oscillator, are presented.

A Nd:GGG crystal of dimensions 18x7x0.5 cm^3, doped at $2x10^{20}$ cm^{-3} Nd^{3+} atomic density, was pumped by up to 40 kW of filtered argon line emission. A small-signal single pass gain (losses excluded) of 1.09 was measured with a probe laser when the DC input to the lamps was 43 kW_e. Our power supply was then modified to operate in a pulsed mode and provided one to three milliseconds pulses at 120 Hz. An average optical output power of 490 watts was obtained at a lamp input power of 93 kW_e in an unoptimized resonator. The laser output power declined after a few tens of seconds since the slab tips were not properly cooled. A birdhouse specular lamp reflector and a contoured diffuse reflector were tested; in both cases the pump illuminated crystal surface was smaller than the total crystal face area. Fluorescence imaging of the zigzag amplifier's output aperture registered a smoother, more uniform pumping profile when the diffuse reflector was used. Uniformity of pumping results in decreased resonator loss and yields higher laser output power. Thermo-optic distortions observed in these preliminary tests are analyzed with the aid of computer simulations of the thermal fields, stresses, and surface displacements of our crystal slab.

2. INTRODUCTION

High average power solid state laser development has been underway at LLNL for most of the past decade. These devices show great promise for applications including laser radar, laser probing of the atmosphere, and tools for cutting, welding and machining hard alloys. They lend themselves to frequency up conversion for still more applications.

Our goal is to obtain a diffraction limited beam of about one kilowatt average power. To reach our objective, we use large, high-quality, neodymium-doped garnet crystals which we must pump to average powers near their fracture limit. High beam quality is achieved in our lasers by optical path length averaging in a zigzag slab geometry.

The zigzag laser architecture was invented[1] by J. P. Chernoch and W. S. Martin at GE research laboratories where it has been effectively employed in aircraft engine manufacture[2]. It has been applied to a number of conceptual designs at LLNL where simulations show its superiority over traditional rod lasers in applications requiring high average power and beam quality. In practice however, the few slab laser examples that exist in the world have not been able to realize high average power and beam quality simultaneously. Rapid, detailed laser experimentation compared to simulation is required to bridge the gap. We have constructed and activated a high average power crystal zigzag laser test bed designed to turn around experiments expeditiously, and have initiated testing a large Nd:GGG crystal amplifier of dimensions 18x7x0.5 cm^3, doped at $2x10^{20}$ cm^{-3} Nd^{3+} atomic density.

Many of the technologies we use must be developed simultaneously, i.e., large neodymium doped crystals, high average power pump sources, reflectors, amplified spontaneous emission absorbing edge claddings, evanescent wave coatings, high average power spectral filters, cooled isolators, cooled Pockels cells, even laser resonator designs. We have used computer codes that have been developed to design these devices and have tried to validate them with experimental data. In what follows, we report the progress we have made in advancing these technologies during the early stages of our amplifier testing program.

3. PUMP SOURCE

The ideal source of upper level activation minimizes heat loading to the laser host. This situation is realized by diode pumping Nd:YAG; however, the average power needed for our design is not yet available from diode lasers although diode development is progressing rapidly. As an alternative, we have chosen the vortex stabilized rare gas arc lamp for the current tests. We purchased two commercially available 20 cm long by 2.1 cm diameter (envelope O. D.) argon arc lamps each rated at 100 kW_e of continuous input power and about 50 kW of optical output power. The Vortek^{TM} lamp achieves unsurpassed average power by cooling the inside surface of the lamp envelope with a spiralling water jet. The full power, continuous output of the two Vortek lamps is excessive for the crystal slabs we are testing; therefore, we have modified the lamps to operate in a simmered, pulsed mode to avoid fracture of our crystals while still generating useful gain.

We have performed absolutely calibrated, high resolution measurements of the characteristic spectra of these Vortek lamps[3] (Fig. 1) and found that 54% of the electrical input is radiated between 200 and 2000 nm. Due to the low current density in the arc (400 A/cm^2) the Vortek lamp spectrum is dominated by lines. Line output between 730 and 830 nm comprises 37% of the total optical output and is well tuned to Nd^{3+}:YAG absorption bands (Fig. 2). The quantum ratio for useful absorption by a 0.5 cm thick slab was found to be 0.69 by convolving the absorption cross section with the Vortek lamp spectrum from 200 to 900 nm. When a spectral filter was used to attenuate the lamp spectral components below 730 nm, the activation of the upper laser level decreased to 86% while the unwanted slab heating decreased to 65% of the levels obtained with the full spectrum. The quantum ratio in the latter case was 0.75 which approaches the quantum ratio expected for diode pumped Nd lasers. These assessments were done for a measured spectrum which only included a restricted range of plasma depths. In our experimental pump cavity, the view factor for transport of energy between the lamp and the slab contains a much broader range of plasma depths and therefore should provide a more thermal spectrum. However, since the plasma is optically thin in the regions away from the lines, our estimates based on spectral measurement are in good agreement with the absorption, heat and quantum ratio that we obtained experimentally in our test amplifier.

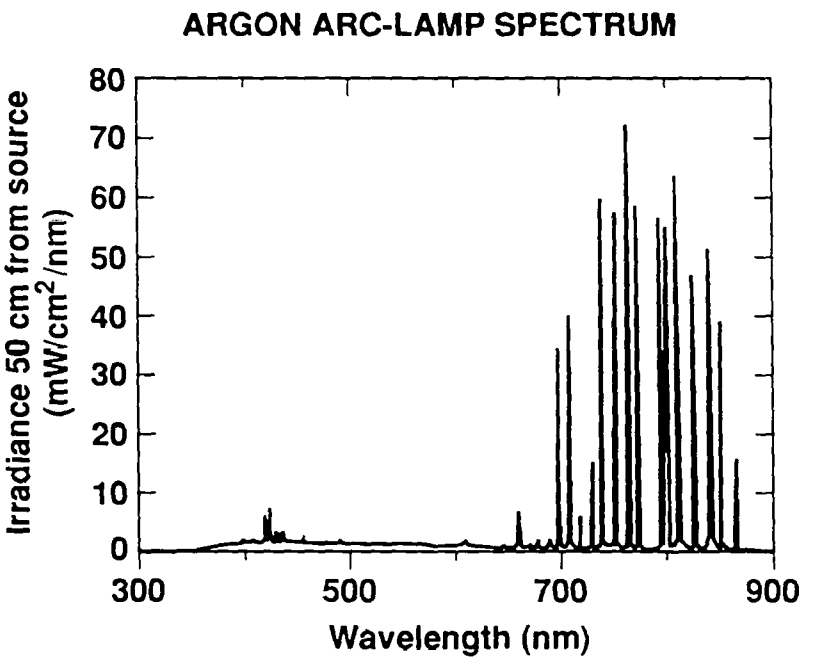

Figure 1. One angstrom resolution spectrum of the Vortek lamp operated at 114 kW_e. The irradiance is absolutely calibrated based on an NBS standard source.

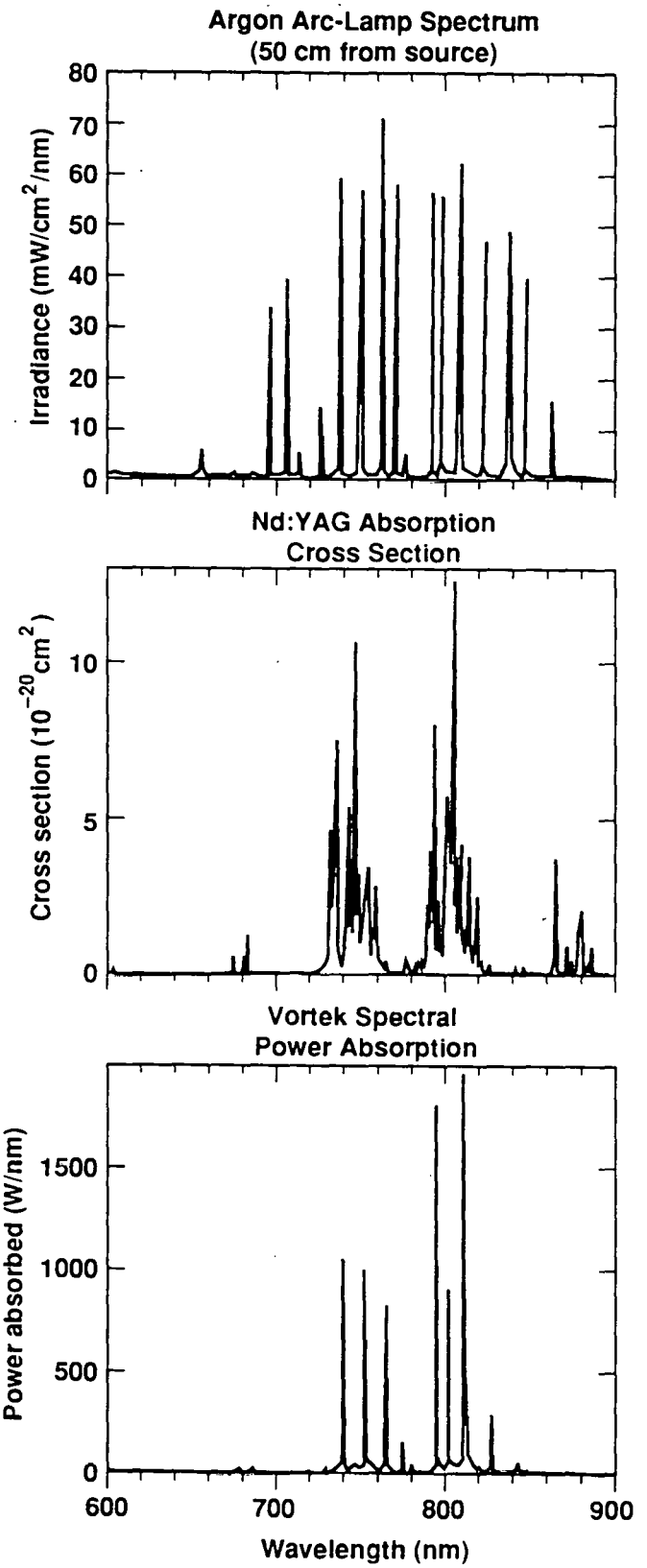

Figure 2. Lamp emission and Nd:YAG absorption. Excellent overlap of emission lines and absorption cross section leads to high pump efficiency.

4. ZIGZAG LASER GEOMETRY AND MATERIALS

Fabricating the gain medium in thin sheets is the most promising route to high average power operation for solid state lasers. The slab geometry combined with zigzag extraction avoids some of the major difficulties characteristic of laser rods. For a fixed volume of gain material, the larger surface area of the slab provides more efficient cooling, and hence lower thermally induced stresses for a given heat load. The stress pattern in the slab also reduces the depolarization of the propagating beam as compared to the rod geometry. In addition, the zigzag optical path made possible by TIR at the large plane surfaces averages gain over depth and eliminates (to first order) thermal lensing across the thickness of the slab aperture. These benefits occur because all ray paths have the same integrated optical properties in a correctly fabricated slab.

Designing a slab for a given performance (power and repetition rate) requires choosing values for many variables (doping, slab dimensions, pump power, etc.) subject to material parameter constraints (thermal conductivity, stress fracture limits, maximum slab size). The detailed optical and thermal physics analysis have been carried out with a suite of computer codes mostly developed at LLNL. Our efforts have added to the available LLNL analytical tools a new computer code for the design of diffuse reflectors and a first order laser kinetic analysis.

Laser materials most seriously considered for our application are Nd:YAG, Nd:Cr:GSGG, Nd:Cr:GGG and Nd:GGG. Intensive research in growth techniques for these materials has been supported by LLNL and others. The material of choice in our modeling is Nd:YAG, however, considerable difficulties have been encountered in the growth of large, core free boules. Very recently, success has been reported by Allied Signal's crystal materials group in growing core free, greater than five cm diameter Nd:YAG boules. The Cr:Nd co-doped materials have an inherent advantage in pump utilization efficiency; however in the case of GSGG, efforts have so far proven only partially successful at simultaneously suppressing spiralling, dislocations and unacceptable optical losses at the laser wavelength. In the case of GGG, Waelker Chemitronic in Germany has successfully grown co-doped material with high optical quality; however, the vastly different segregation coefficient for the two ions in GGG has rendered these boules unusable (green at one end, pink at the other). The segregation problem may be solved in the future through melt replenishment or by using a large crucible.

Owing to its popularity as a substrate material for bubble memories, GGG was developed during the 70's and can be grown to a diameter of 15 cm with high optical quality. The lattice parameter of the substitutional Nd^{3+} sites is such that it accepts the lasant ion without stressing the lattice; consequently, Nd:GGG can be doped highly (up to 4.5×10^{20} ions/cc, the half lifetime doping). A major problem encountered with Nd:GGG has been solarization (formation of color centers) after irradiation with wavelengths below 480 nm. Waelker Chemitronic claims to have recently solved this solarization problem using a proprietary process. Our boules were grown by Allied and the slabs were fabricated by Zygo. We prevent solarization by using a high average power spectral filter consisting of a solution of potassium dichromate $K_2Cr_2O_7$ directly added to the slab coolant water. The solution is chemically stable and has protected our slabs for several months with over 3 hours of integrated high power pumping. As was pointed out in the previous section, the estimated penalty for using such a spectral filter is modest because the upper laser level activation decreases by less than 1/6 while the heat loading decreases by more than 1/3. The measured transmission for a sample of the cooling solution is less than 0.2% at wavelengths below the solarization threshold of 486 nm (Fig.3). The measured transmission in the intended pump bands from 700 to 850 nm exceeds 97% in the 3 mm depth of the coolant channel.

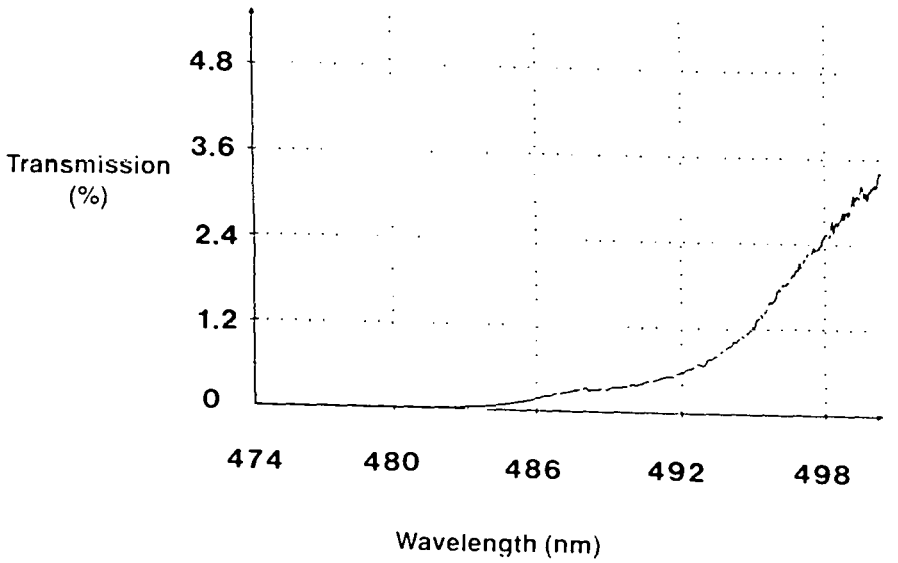

Figure 3. Measured transmission in a 3 mm path sample of the potassium-dichromate/water coolant solution.

5. MECHANICAL DESIGN

5.1. Evanescent wave coating

The high average power laser beam reflecting internally on the large faces of the slab will couple into materials in contact with these surfaces either evanescently or refractively. If the evanescent wave were allowed to penetrate the turbulent coolant flow, their interaction would add a random component to the phase front which would be translated into an optical diffractive loss. Another issue is how to seal the coolant flow without risking optical damage at the sealing surface. We have developed an evanescent wave coating which allows the coolant and the sealing O-rings to be in contact with the large pumping/cooling faces of the slab. It consists of an evaporated coating of SiO_2. After a few trials with different thicknesses, we settled on a coating thickness of one micrometer. At this thickness, the coating is mechanically stable and is not destroyed when compressed against the sealing O rings. As an added benefit, we have chosen the thickness to act as an AR coating (at near normal incidence) for the pump bands about 810 nm. At the internal angle of incidence of the laser beam, the extinction is five e-foldings in amplitude, practically isolating the TIR surface from the cooling/sealing surface.

5.2. Laser head, coolant flow hardware

The laser head (Fig. 4) contains the crystal slab, the pump windows, and the cooling channels and plenums. The slab is positioned such that the pump faces are vertical, and its weight is supported at the wedged tips only. These supports are made of silicone rubber and also act as seals for the liquid coolant. The laser head is mounted on a rigid support structure which also supports the resonator optics and optical diagnostics. The water cooled reflectors are mounted on the Vortek lamps. The reflector apertures are positioned within 0.5 mm of the laser head pump windows to avoid contact. This is done to isolate the laser head from vibrations in the Vortek lamp caused by high velocity water within the arc envelope.

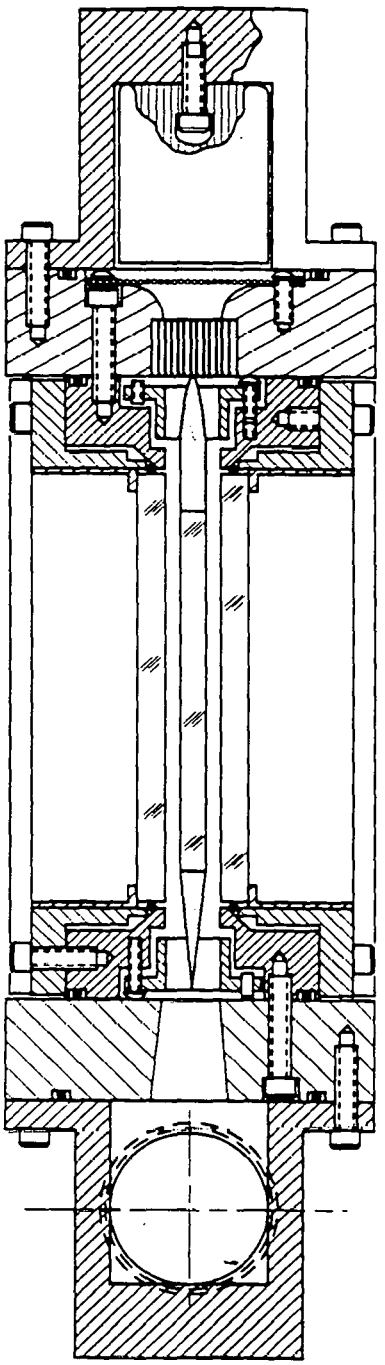

End on View

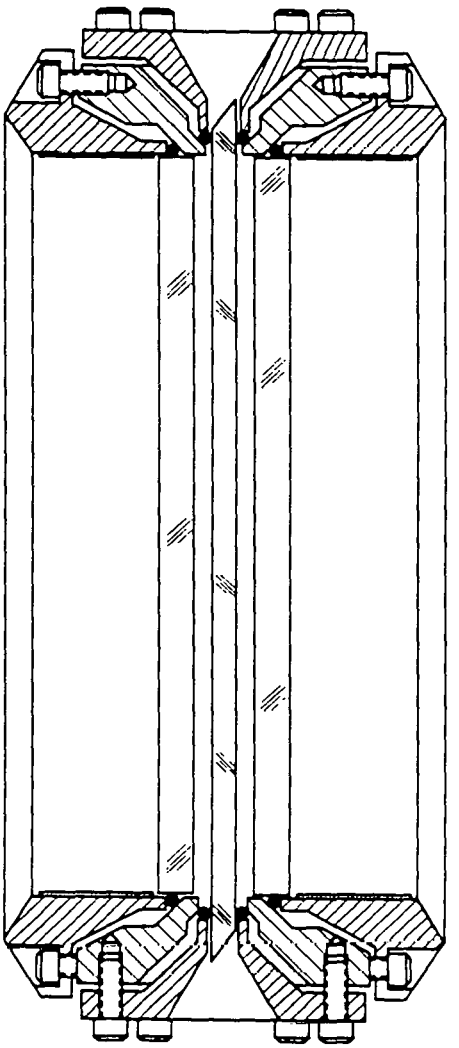

Top Down View

Figure 4. Laser head. Hardware details.

The slab faces are convectively cooled with potassium dichromate doped water. The cooling system is designed to remove 100 kW from the laser head, the maximum optical power output of the two Vortek lamps. The maximum allowable temperature rise for the coolant is 5^{o} C for a volume flow rate of 4.7 l/s (75 gpm). At this flow rate, the water velocity in the cooling channel is 5.1 m/s corresponding to a Reynolds number of $3x10^{4}$. The coolant enters the head through two pipes into a tapered manifold. The coolant is then turned 90 degrees into a curved contraction, through a fine mesh screen and honeycomb flow conditioning section. The flow splits into two independent channels with half going up each side of the slab. The two flow channels recombine at the end of the slab in an exhaust diffuser which dumps into a tapered exhaust plenum. The coolant exits the laser head at the ends of the slab through two pipes.

In order to diagnose the coolant flow, a stream of nitrogen was injected. A homogeneous bubble flow was visible with no eddies or stagnation regions anywhere along the slab cooling faces.

6. REFLECTOR

A most important component in a high average power slab laser is the reflector. The transport of lamp energy by the reflector to the slab volume gives rise to the gain and heat source distribution. This source drives the distributions of temperature and stress, and the surface deformations. If beam quality calculations are desired, the pumping profile must be predictable. The reflector geometry can be tailored to provide the desired source distribution. It is thus very important that codes used for reflector design be validated by experimental measurements. Both a "birdhouse" specular lamp reflector and a contoured diffuse reflector were tested and compared to design code predictions.

6.1. Specular reflector

The specular reflector was designed with the aid of MIR3D, a three-dimensional ray tracing Monte-Carlo code written at LLNL for a CRAY computer. This code attempts to account for all surfaces, absorbers and leaks for rays of two types of spectral emission/absorption properties; i.e., high opacity and low opacity rays. The design is made up of four flat mirrors around the lamp and two flat mirrors at the ends with holes through which the lamp is inserted (Fig. 5). The source distribution desired at this stage of development is a flat distribution which the code provided to within 5%. Two reflector housings were built of cooled aluminum plates. To avoid degradation of the reflecting surface, second surface mirror glass (low iron glass to avoid UV absorption) was used, with its coated side contacted to the cooling plates.

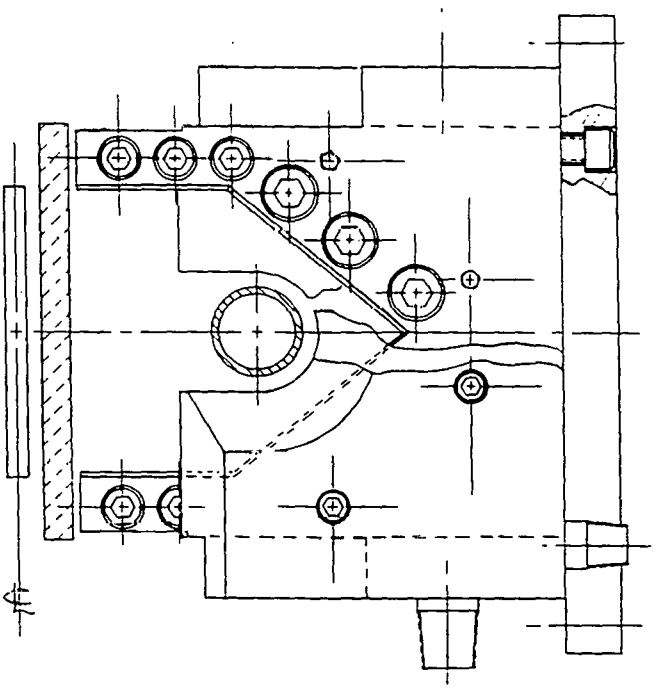

Figure 5. Second surface mirrored glass is contacted to the cooled surfaces of this specular "birdhouse" reflector design.

6.2. Diffuse reflector

The diffuse reflector was designed with a new two dimensional code which combines ray tracing and a number of physical assumptions related to lamp emission properties (surface radiator, perfect absorber), wall reflectivity (Lambertian), slab absorption (computed from experimental emission and absorption spectra), and symmetry (only one quadrant of the reflector is worked on). An optimizing algorithm alternatively varies the parameters of a cubic equation converging on a reflector profile on the basis of the least squares value between the desired pumping profile and that obtained in successive runs. A reflector profile was designed with predicted pump uniformity within 2% over 90% of the slab surface. As a diffuse reflectance material we chose Spectralon^{TM}. This material is used in integrating spheres; the manufacturer claims a reflectivity greater than 99% at 800 nm. We tested one cm^2 samples of this material, and found them to resist a radiant flux of 500 W/cm^2 (the outside surface of the lamp). Diffuse reflectors were built by cutting the designed profile by wire electric discharge machining (EDM) from solid aluminum blocks and drilling cooling channels beneath the surface profile (Fig. 6). A thin sheet (3.2 mm) of spectralon was then glued to this surface using a high temperature silver epoxy.

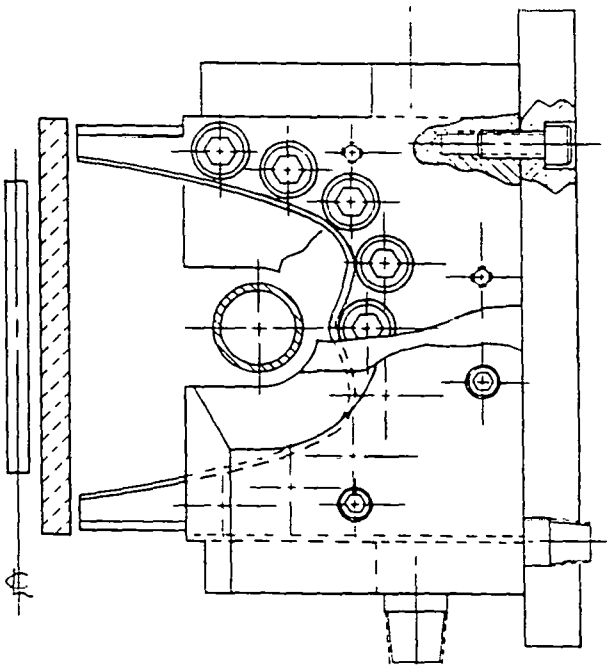

Figure 6. Highly reflective material (Spectralon) is glued to the cooled surface of this contoured diffuse reflector design.

6.3. Reflector test results

A diffuse reflector is inherently forgiving of high frequency modulations, spatial fluctuations of the source, etc., such as may be expected from a real plasma arc. Its shortcoming is the transport efficiency since every ray reflects off the reflector wall more times per transmission through the slab than in a specular reflector. This disadvantage is countered by the higher reflectivity of spectralon (99%) than most specular reflectors (90-97%). As the wall reflectivity approaches unity, the source must find its way to the remaining sinks: leaks, the slab and the lamp plasma. The leaks can be minimized by proper engineering, ideally leaving the slab to absorb pump light and the lamp plasma to re-absorb the balance of the spectrum.

We do not have quantitative data on the relative transport efficiency merits of both types of reflector as of yet. Fluorescence imaging of the zigzag amplifier's output aperture registered a smoother, more uniform pumping profile when the diffuse reflector was used (fig. 7). Uniformity of pumping results in decreased resonator loss and yields higher laser output power. This has been evidenced by laser output data which showed a factor of 1.5 increase in output power under otherwise identical conditions when our specular reflectors were replaced with the diffuse reflectors.

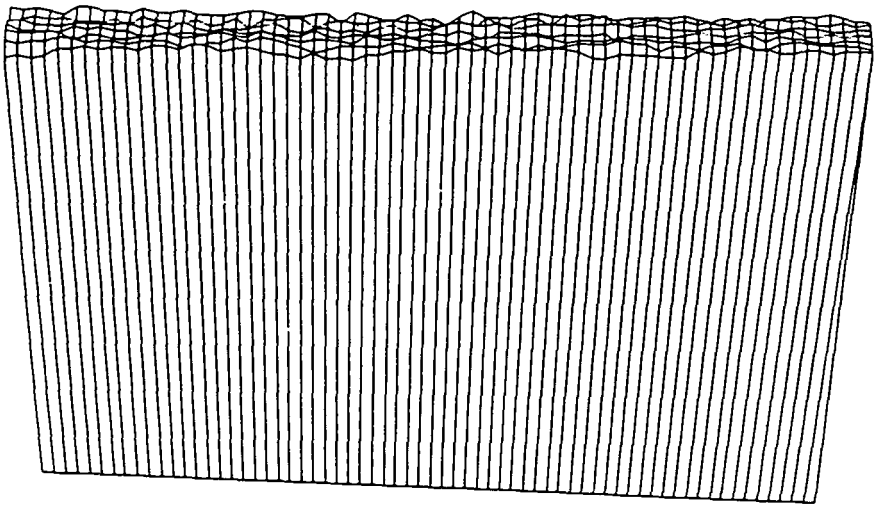

Fluorescence intensity profile – diffuse reflector

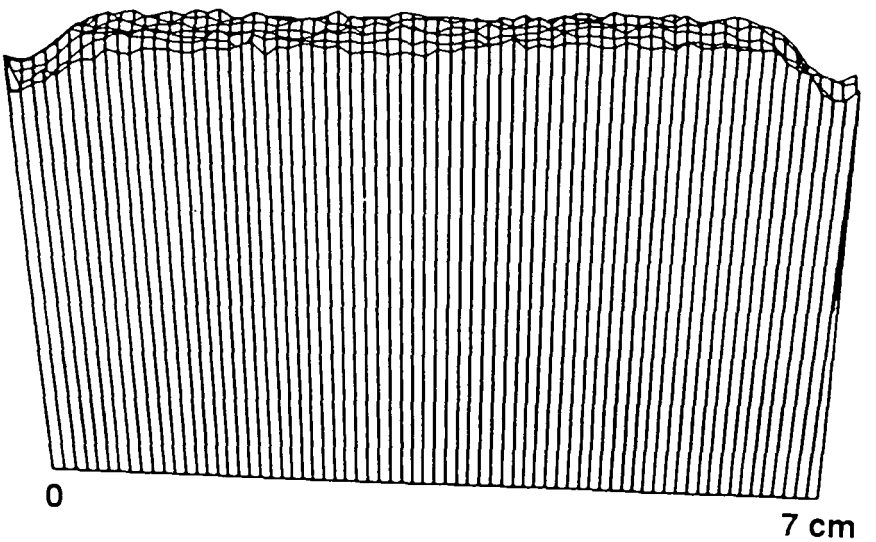

Fluorescence intensity profile – specular reflector

Figure 7. Lineouts of the fluorescence imaging experiments. The roll-off at the edges is evident for the specular reflector.

We have experienced reflector failure at high average powers. In both types of reflectors, the failure could be tracked back to contamination at some surface within the pump cavity. Neither has failed below about 50 kW_e of total input power. In the case of the specular reflector, a conductive grease used to contact the mirrored glass to the cooling plates evaporated, apparently because of hot spots in the cooling system. The vapor found its way to the inside of the pump cavity, plating on the inner surface and causing fracture of the glass. In the case of the diffuse reflector, a similar failure mode was experienced in the end plates which were specular second surface reflectors. When the end plates were replaced by spectralon, failure occurred at 94 kW_e apparently due to impurities within the bulk of the spectralon material.

7. EXPERIMENTAL LASER DATA

Most of the initial activation of the crystal laser test bed has been dedicated to troubleshooting the concurrent technologies. Laser data has been scant but encouraging.

7.1. Gain measurement

As a probe laser, we used a diode pumped cw Nd:GGG mini-laser built by Amoco Laser Co. to operate on a single spectral line (1.0622 mm) and 2 to 3 longitudinal modes. Two chopped pyroelectric detectors fitted with narrow band filters and a ratiometer were used for gain measurements. The collimated 3 mm diameter beam was sampled with a beam splitter and then transmitted through the center of the slab aperture. After one zigzag pass through the slab, the beam was sampled again, and the ratio of the signals was set to unity with the Vortek lamps off. With the Vortek lamps operating continuously, the fluorescence background signals were registered with the probe beam blocked, allowing correction of the probe laser signals before they were ratioed at each power level. The natural logarithm of this ratio is then the small signal gain as a function of the power input. A straight line fit to the data is presented in Fig. 8. The slope of the fit is 0.0026/kW_e.

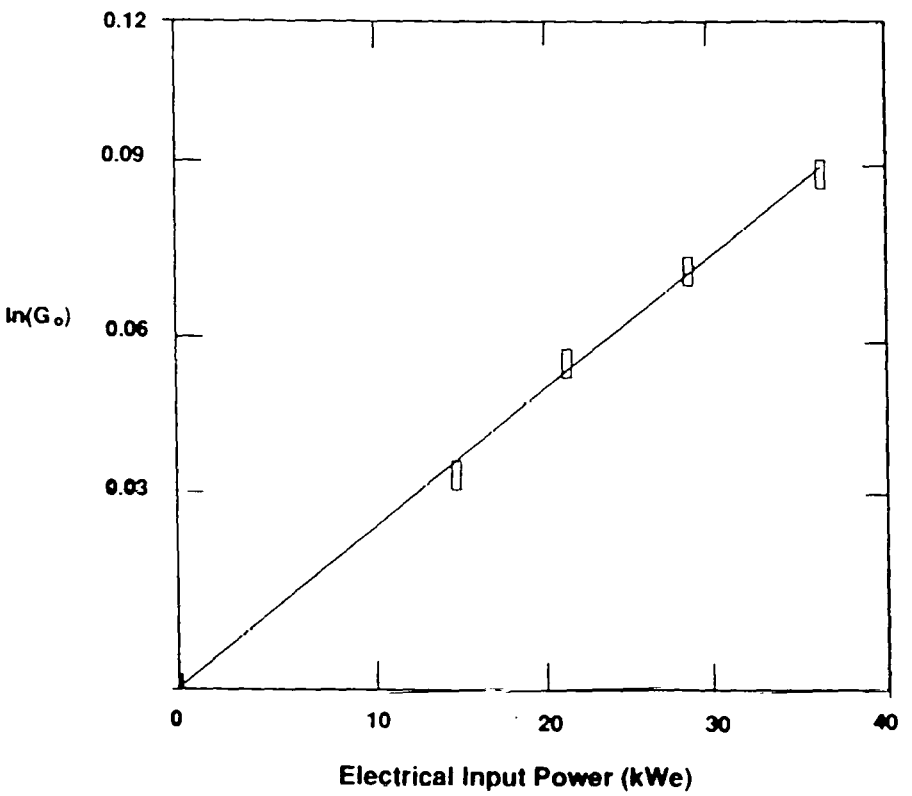

Figure 8. Straight line fit to the small signal gain data. The intrinsic loss/pass of 3% is included. The slope is 0.0026/kW_e within the pump cavity (the lamp arc is 33% longer than the reflector cavity).

7.2. CW output power

A flat-curved resonator was used for initial laser extraction experiments. The 5 m curvature high reflector and a flat output mirror were placed approximately one meter apart. The "birdhouse" specular reflector was used. A calorimeter was used to collect the emerging beam. The leakage at the high reflector was split so that the output beam could be projected and recorded by a CID camera as well as temporally resolved by a silicon detector fitted with a narrow band filter.

In cw experiments with a 95% output coupler, threshold onset of lasing was found at 25 kW_e input power. Laser output was not stable. It reached approximately 100 W output at 50 kW_e input decaying to 10 W output after only 10 seconds. This behavior was attributed to uncontrolled heating of the slab tips which were not cooled in our original design. Gold foil was then contacted to the inside of the laser head window shadowing about 19 mm at each end of the flow channel. This introduced cooled areas between the pumped region and the slab tips. The gain length and gain to loss ratio were reduced by this shading, and the laser output power was then a lower, but steady 35 W at 50 kW_e input for several minutes with no signs of decay.

7.3. Pulsed operation

The Vortek lamps were modified to operate in a simmered, pulsed mode by disconnecting one phase in the three phase SCR bridge and bypassing the inductor. Quasi-sinusoidal pulses were obtained at 120 Hz with widths of 0.5 to 4 ms depending on the phase controller delay. This resulted in a higher gain to loss ratio at extraction time while holding the average power within the thermal fracture limits of the slab. The higher gain to loss ratio improved the extraction efficiency of the laser oscillator.

The reflector cavity length was 15.3 cm. With a 90% output mirror and diffuse reflectors, the average output power peaked at about 150 W before settling at 90 W after about 10 seconds and remaining stable for as long as 13 minutes. The peak and average input powers were 180 kW_e and 47 kW_e, respectively. At higher average input powers, the output would never settle at a specific output, oscillating wildly over factors of two to three with a time constant of about 5 seconds (about the response time of the calorimeter). The highest average laser output we observed was 490 watts obtained with an 80% output coupler at peak and average input powers of 280 kW_e and 93 kW_e, respectively.

The output power at any input pump power was predictable and fit a first order kinetic model. The characteristics of the pumping pulses varied for every power level, but were slow compared to the kinetics of the laser ion and therefore in equilibrium with the pump. Table I shows the results of the experiments with the 80% output coupler and the predicted output using a Rigrod model integrated over a pumping pulse with characteristics similar to those obtained experimentally. The results show reasonably close agreement. Figure 9 shows a typical oscillogram of the input/output waveforms when the input was 256 kW_e peak and 72 kW_e average. A typical image of the near field obtained is displayed in Fig. 10.

Table I. Pulsed pumping results, fit to rigrod model.

INPUT POWER (kW_e)		PULSE SHAPE (ms)		OUTPUT (W)	
Peak	Average	Risetime	Width	Experimental	Model
100	26.2	1.5	2.0	15	21
182	47.2	1.3	2.5	155	168
256	72.0	1.6	3.5	400	412
288	94.0	1.9	4.5	490	493

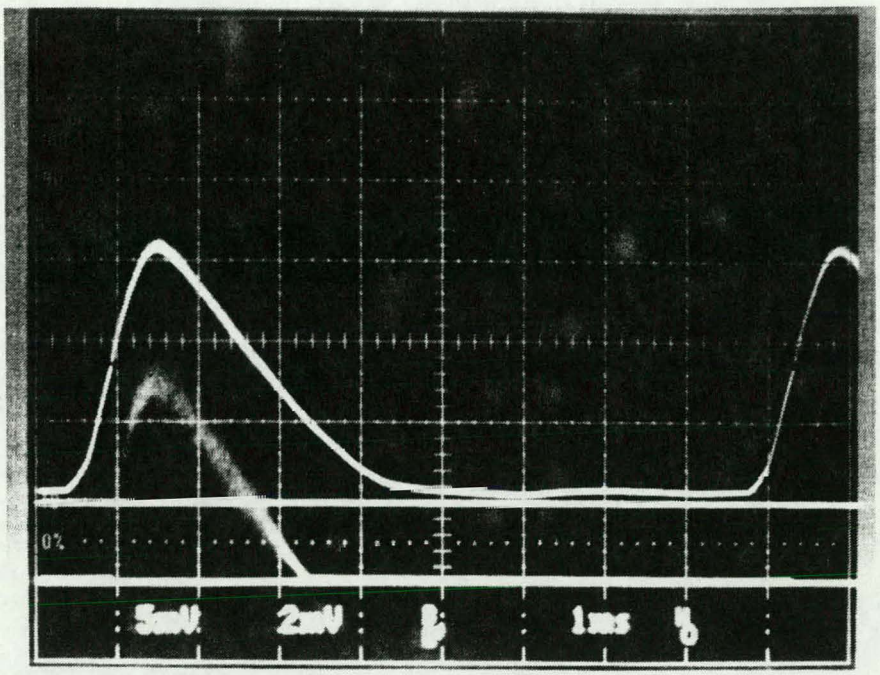

Figure 9. Typical oscillogram of the Nd:GGG oscillator. The bottom trace is the laser output. The top trace is the lamp output.

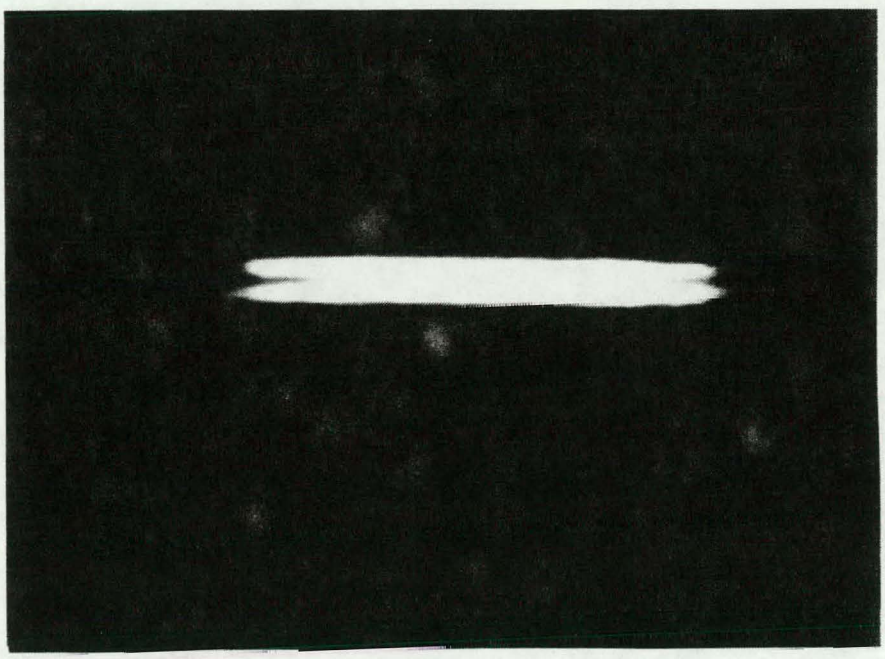

Figure 10. Near field image of the output laser beam. In the thin dimension, the beam profile is indicative of a low order laser mode. In the long dimension, no structure can be discerned from these data; however, during the experiments, mode hopping of higher order modes was visually apparent.

8. THERMO-OPTICAL DISTORTIONS MODELING

The Tecate-Brew family of 3-D codes was used to analyze the slab performance for several experimental conditions. These codes first solve the energy equation to determine the slab temperature distribution as a function of time with 93 kW_e total power input to the lamps. The results are used to calculate the strains and stresses at a particular time (40 s in these calculations; steady state appears to be achieved by 10 s in most cases). Finally, the temperatures, strains and stresses are used to determine the phase and depolarization of a beam propagating though the zig-zag slab using geometric ray tracing.

The temperature code has the capability to accept source function input from our 3D Monte Carlo ray trace code, MIR3D. However, we instead chose to use an idealized source function to facilitate zoning, use of a new diffuse reflector material, and adjustment of the source function using experimentally determined results. The idealized source was a "cone model" with a cone originating at each element's centroid; the cone angle is determined by Snell's law, and the cone's intersection with the surface specifies the region contributing to the local interior source function. The surface source was a uniformly distributed Labertian, and it was truncated at specified locations.

For the diffuse reflector, we used the cone model truncated at the slab edge. The 2D reflector design code indicates some small variations in uniformity, and the reflector was built over-sized to reduce the source droop near the slab edges. The specular reflector was not over-sized, and its surface source uniformity was overlaid with a variable mask (along the TIR surface's short dimension) that corresponded to the 1-D distribution of fluorescence in the experiments. The mask resulted in "eyes" in the calculated interferograms for the specular reflector (Fig. 11a), and these features were also observed in experimental interferograms.

For both reflectors, when the cooling length was set to the reflector cavity length, the standoff of the reflector from the slab (due to the window and coolant thicknesses) caused the heat source to extend into the uncooled ends. The ends became very hot and warped, and the calculated wavefront was unacceptable (>10 waves in the long dimension after one slab thickness was eliminated from each end, 3.3 waves in the thin dimension). In addition, the location of the heat transition caused a phase shift near the center of the beam's thin dimension; this shift was confirmed by the lack of extracted beam in this region in oscillator experiments when the diffuse reflector was used (compare Fig. 11b with Fig. 10).

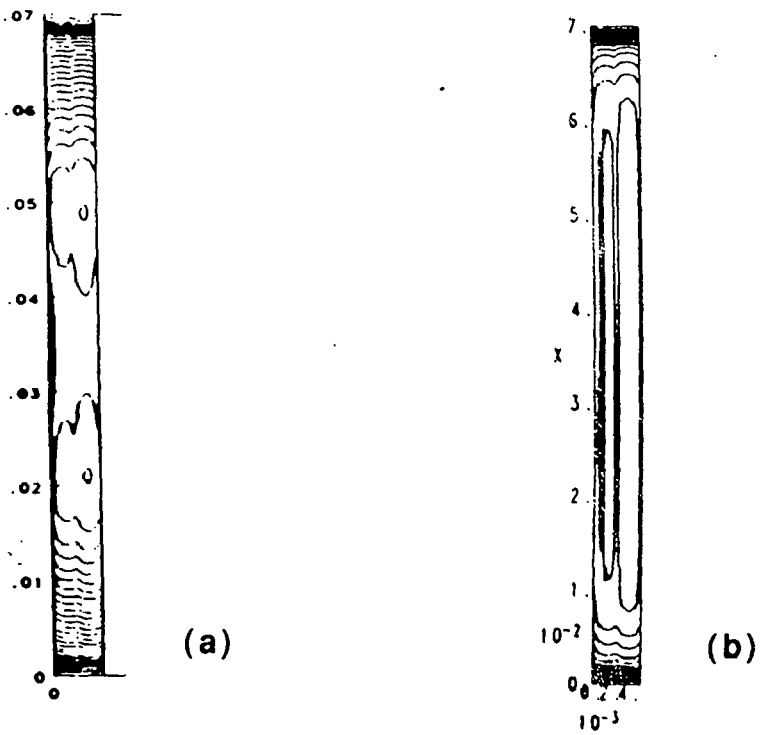

Figure 11. One wave phase error contours calculated for the tailored pumping profile (a), and the homogeneous pumping profile (b).

The obvious improvement was to extend cooling over a larger region of the TIR surface. The hardware was modified to cool the entire TIR surfaces with turbulent 20°C water. The calculated wavefront improved for both reflectors, to 1.1 waves in the thin dimension and to 7.3 and 37 waves in the long dimension for the diffuse and specular reflectors, respectively. In the long dimension, elimination of two (rather than one) slab thicknesses at each end would remove most of the aberration. Alternatively, the source function must be prevented from drooping at the slab edges.

Although the fully cooled results were a distinct improvement, it was clear that much of the remaining distortion was due to the overcooled ends. A series of runs for the diffuse reflector used a heated water coolant on the ends of the TIR surfaces; temperatures of 48, 55, 62, and 66.7°C were used (66.7°C was the thickness-averaged temperature of the pumped region of the slab). The thin-dimension wavefront dropped to 0.7 waves for the 48°C coolant and then increased to 0.9, 1.2 and 1.4 waves as the temperature was further increased. The slab end deformation passed from shrinking to growing between the 55 and 62°C cases, indicating that the wavefront is influenced by the transition region as well as by the end conditions.

The best wavefront is shown in Fig. 12. Of the three material properties affecting the wavefront, the phase is affected most by dn/dT (about 2/3 of the total), less by the coefficient of thermal expansion, and negligibly by the stress-optic coefficients. The next planned computational improvement is to more smoothly vary the TIR coolant temperatures.

Figure 12. Simulated interferogram for the diffuse reflector with 48°C end coolant temperature. One slab thickness has been removed from each end. The contour interval is 1/2 wave.

9. CONCLUSIONS, FUTURE PLANS

The crystal laser test bed has been activated and encouraging laser data have been obtained. The next iteration will include new pulsers for the Vortek lamps which should provide better gain medium characteristics for improved extraction, improved thermal management hardware at the slab tips and argon gas flooding of the reflector cavity to prevent degradation or darkening of the spectralon material. In the near future, we will continue work on alternative reflector designs and materials in our effort to make the zigzag crystal laser achieve its potential of high average power with diffraction limited performance.

10. ACKNOWLEDGEMENTS

This work performed under the auspices of the U. S. Department of Energy by the Lawrence Livermore National Laboratory under contract number W-7405-ENG-48, for the U.S. Army of MIPR No. W31-RPD-63-A072.

11. REFERENCES

1. W. S. Martin, J. P. Chernoch: U.S. patent No. 3633126 (Jan. 1972).

2. H. Heckler, "Expanding the Frontiers of Laser Applications," Industrial Laser Review, October 1989.

3. L. E. Zapata, "Absolute Intensity, High Resolution Spectrum of the Vortek Arc Lamp and Its Spectral Match to Nd:YAG Bands," LLNL internal report: UCID-21703, May 10, 1989.

Technical Information Department · Lawrence Livermore National Laboratory
University of California · Livermore, California 94551

DO NOT MICROFILM
COVER